JOURNAL OF APPLIED PHYSICS **103**, 014503 (2008)

Time-of-flight studies on $TiO_2/CuInS_2$ heterojunctions

Joris Hofhuis[a),b)]
Opto-Electronic Materials, Delft University of Technology, Julianalaan 136, 2628 BL Delft, The Netherlands

Joop Schoonman
Delft Institute for Sustainable Energy, Delft University of Technology, Julianalaan 136, 2628 BL Delft, The Netherlands

Albert Goossens[b)]
Opto-Electronic Materials, Delft University of Technology, Julianalaan 136, 2628 BL Delft, The Netherlands

(Received 20 September 2007; accepted 24 October 2007; published online 4 January 2008)

Time-of-Flight (TOF) measurements have been performed on *n*-type TiO_2/*p*-type $CuInS_2$ heterojunctions. The TiO_2 film thickness has been varied between 200 and 400 nm, while the $CuInS_2$ film thickness has been fixed at 500 nm. The TOF response can be accurately modeled, if the potential drop across the *p*-*n* heterojunction with a large density of interface states is properly accounted for. Also electron transport in a space-charge region for a not fully depleted semiconductor has to be considered. The electron mobility in TiO_2 is found to be 10^{-2} $cm^2\ V^{-1}\ s^{-1}$, independent of the TiO_2 layer thickness. The interface-state densities are 5×10^{11}, 2×10^{12}, and 6×10^{12} $eV^{-1}\ cm^{-2}$ for 200, 300, and 400 nm thick TiO_2 films, respectively. © *2008 American Institute of Physics*. [DOI: 10.1063/1.2826685]

I. INTRODUCTION

In order to reduce the energy payback time and the production costs of solar cells, alternative materials and device concepts need to be developed. In the past years, research in our laboratory has been focused on the development of all solid-state three-dimensional (3D) solar cells,[1–3] in which *n*- and *p*-type semiconductors are blended on a nanometer scale. Nanocomposites of anastase TiO_2 and $CuInS_2$ (CIS), with In_2S_3 as a buffer layer, exhibit an energy conversion efficiency of about 5%.[2] Since these solar cells have been obtained by spray pyrolysis in air at a substrate temperature of about 300 °C, the economical potential for this device concept has been demonstrated convincingly. Spray pyrolysis[4–8] is a simple technique open to large-scale production of thin-film solar cells. Obviously, the material quality is less than that obtained with more advanced technologies and relative high defect concentrations can be expected. Defects in $CuInS_2$, i.e., interstitials, vacancies, impurities, and antisites defects (copper-gold ordering), have a negative effect on the energy conversion efficiency, since they reduce the lifetime and mobility of the charge carriers.[9]

In chalcopyrite-based photovoltaic devices, a heterojunction between the chalcopyrite-structured absorber and the *n*-type buffer material is formed. Formation of a heterojunction can give rise to interface states, which reduce the efficiency of the device when energy levels are located in the band gap of the light-absorbing material. When the interface state concentration is high, Fermi-level pinning may occur, which affects the internal electric field at the junction.[10,11] Not much is known about the influence of interface states on the charge carrier transport in chalcopyrite-based solar cells. The present study is directed to elucidate the relationship between the density of interface states and the charge carrier dynamics in $TiO_2/CuInS_2$ heterojunctions using the time-of-flight (TOF) technique. In TOF, a short laser pulse creates charge carriers at the $TiO_2/CuInS_2$ junction, which drift away from the junction region by the internal electric field. The mobile charges are detected using two nonblocking electrodes. In this way, the samples under investigation are solar cells and the outcome of TOF experiments is closely related to the transport of carriers in solar cells under operational conditions.

The magnitude of the internal electric field at the local junctions in nanocomposites is difficult to determine. Therefore, in the present study thin-film bilayer devices are investigated instead of 3D nanocomposites.

A. Time-of-flight background

With the time-of-flight technique, the transport time of a sheet of charge carriers through a material is measured.[12] Charge carriers, which are generated by laser-induced excitation, drift through a sample between the electrodes under the influence of an applied electric field. If the width of the sheet of charge carriers is small compared to the thickness of the film, the carrier transit time can be detected. The width of the sheet of charge carriers is related to the duration of the laser pulse and is broadening somewhat during the flight.[13] The transit time τ is defined as the moment when half of the charge carriers has crossed the sample. In the simplest case, the mobility follows from:

[a)] FAX: +31 15 278 7421. Electronic mail: j.p.t.hofhuis@tudelft.nl.
[b)] Also at: Delft Institute for Sustainable Energy, Delft University of Technology, Julianalaan 136, 2628 BL Delft, The Netherlands.

$$\mu = \frac{v}{E} = \frac{d/\tau}{E}, \tag{1}$$

where μ and v are the charge carrier mobility and velocity, respectively, E is the electric field, d is the sample thickness, and τ is the transit time. A relation between the transit time and the electric field can be derived from Eq. (1),

$$\frac{1}{\tau} = \frac{\mu}{d}E = \frac{\mu}{d^2}V, \tag{2}$$

in which V is the applied bias, which in this approximation decreases linearly over the thickness of the sample. A plot of $1/\tau$ as a function of V will show a straight line of which the slope relates to the mobility of the charge carrier.

Several important conditions need to be fulfilled in a well-performed time-of-flight experiment. First, the generated charge should be much less than the surface charge on the electrodes to ensure that the internal electric field is not affected by the injected charge carriers.[12]

Second, to freeze-in slow dielectric relaxation, the direct current (dc) voltage must be applied just before the laser pulse.[12] Third, the response time of the electrical measurement system (including the sample) must be less than the transit time. If not, the measured current response is affected by the instrumental bandwidth.[12] Fourth, changing the thickness of the film should not affect the derived carrier mobility when nondispersive transport is considered.

B. Time-of-flight on *pn*-heterojunctions

The aim of this work is to measure the transport of charge carriers in n-TiO_2/p-$CuInS_2$ heterojunctions. In contrast to conventional TOF experiments, two semiconductor materials, instead of one, are involved. However, if one of the two semiconductors has a much higher charge carrier mobility than the other, it merely acts as an electrical contact for the semiconductor with the low charge carrier mobility. In that case, the only difference with the normal TOF experiment is, that the applied voltage is divided over both semiconductors, which implies that the local electric field is not simply V/d. To determine which of the two semiconductors has the lowest charge carrier mobility, the film thickness of both layers has been varied. It appears that in $TiO_2/CuInS_2$ heterojunctions the electron mobility in TiO_2 is much smaller than the hole mobility in $CuInS_2$. By measuring the electron transit time in TiO_2 it is possible to assess the voltage distribution in $TiO_2/CuInS_2$ heterojunctions, which depends strongly on the electronic properties of the $TiO_2/CuInS_2$ interface.

To relate the measured transit-time values with the applied bias voltage and the film thickness, a model of the $TiO_2/CuInS_2$ heterojunction has been elaborated, which is further discussed later.

II. EXPERIMENTAL ASPECTS

Both the TiO_2 and the $CuInS_2$ films have been deposited on SnO_2-coated glass substrates (TCO) using automated aerosol spray pyrolysis. More information about the synthesis of TiO_2 and $CuInS_2$ can be found in Refs. 4–8. The backcontact is a vacuum-evaporated disk of gold with a diameter of 2 mm. Carbon paint is used to make electrical contact with the TCO front electrode. Three samples have been investigated, in which the $CuInS_2$ layer thickness is kept at 500 nm and the TiO_2 thickness was varied, i.e., 200, 300, and 400 nm. Figure 1 schematically describes the time-of-flight setup. A Nd-yttrium-aluminum-garnet laser (SpectraPhysics QCR) operating at 355 nm, 7 ns pulse width, and 10 Hz repetition rate, pumps a MOPO (SpectraPhysics MOPO 710). After passing through several neutral density filters and a pinhole, the energy of the pulse is 0.5 $\mu J/cm^2$. A fast photodiode is used to trigger the detecting electronics. A pulse generator (Agilent) provides the voltage pulse. The exact timing of the applied voltage pulse is set using the delay option of the pulse generator. An oscilloscope (Tektronix TDS 744), being triggered by the photodiode, records the photocurrent through its internal 50 Ω resistance. To measure the dark current at the applied voltage an electronic shutter is closed. The samples are mounted in a liquid-nitrogen cooled cryostat (Oxford Optistat DN) for stabilizing and varying the temperature.

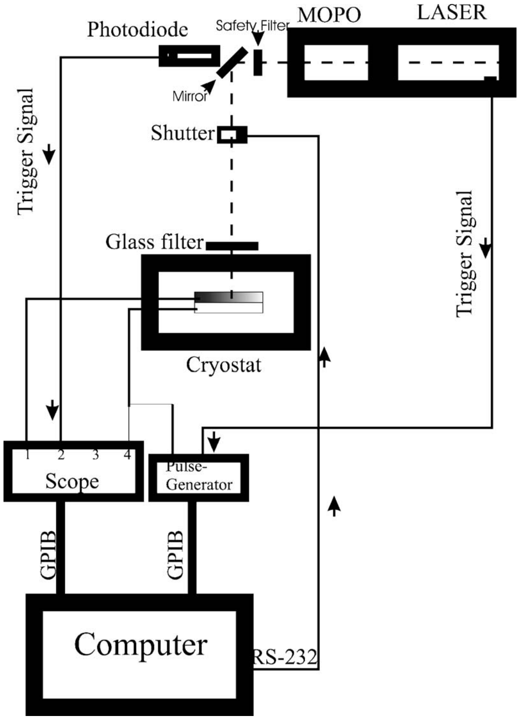

FIG. 1. Schematic representation of the TOF setup. The solid lines represent electrical wiring. The dashed line represents the laser path. The sample is mounted in a LN-cooled cryostat. The complete experiment is computer controlled.

III. RESULTS

Figure 2 shows a typical current-voltage (I-V) curve in the dark and under illumination for a $TiO_2/CuInS_2$ heterojunction with a TiO_2 thickness of 300 nm. The sample shows good diode behavior with a rectification ratio at $+/-1$ V of 10^3. Charge extraction experiments have been performed. In these experiments, the bias voltage is set at 0 for some time. At $t=0$, the bias voltage is stepped to a reverse bias (i.e., -1 V) and the current transient is measured. The current

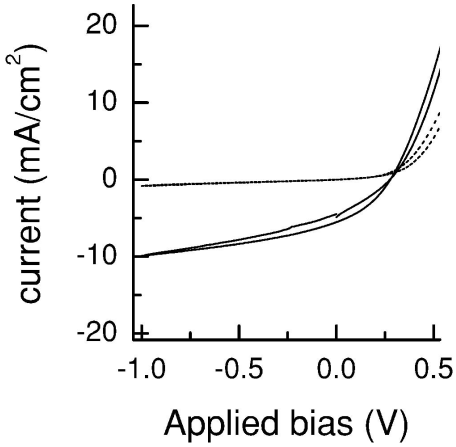

FIG. 2. *I-V* curves for the 300 nm TiO_2 sample in the dark (dashed line) and under illumination (solid line).

response shows an exponential decay with a time constant of 10^{-6} (s), as shown in the inset of Fig. 3. The area under the curve represents the extracted charge, which is plotted in Fig. 3 as a function of applied bias. A linear relation between the extracted charge and the applied bias is found. The ratio between the extracted charge Q and the voltage V, i.e., $\Delta Q/\Delta V$ is the cell capacitance, which is 8×10^{-7} F/cm^2.

Figure 4 shows a TOF photocurrent response on a linear scale. The TOF response shows only a very weak temperature dependence between 260 and 310 K. The area under the TOF curve represents a charge of 10^{-10} C. For a 300 nm thick sample, with a diameter of 2 mm, the injected charge density amounts to 10^{14} cm^{-3}, which is well below the donor density in TiO_2 of about 10^{17} cm^{-3}. Accordingly, the injected charge carriers do not disturb the internal electric field. As can be seen from Fig. 4, it is impossible to determine the transit time from this graph in a direct way. Figure 5, therefore, shows the same transient on a log-log scale. The transit time is indicated in the figure. Plots of $1/\tau$ as a function of the applied dc bias are presented in Fig. 6 for all three samples at a temperature of 290 K. For voltages less than 1.5 V the transit time is almost independent of the applied bias. For voltages above 1.5 V, $1/\tau$ is voltage dependent, but the voltage and the film thickness dependence do not follow Eq. (2). Furthermore, the transit time changes with the TiO_2 layer thickness and does not change upon variation of the $CuInS_2$ layer thickness (not shown). We conclude that the current response is related to the transport of electrons in TiO_2.

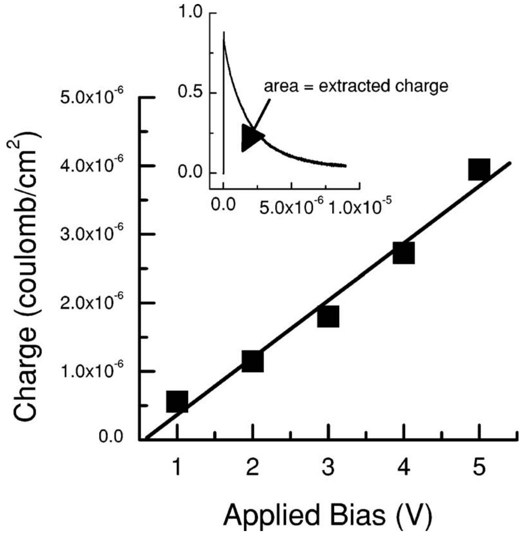

FIG. 3. Charge extraction measurements. Extracted charge for a 300 nm thick TiO_2 sample. The inset shows the current response after applying a bias step of 2 V.

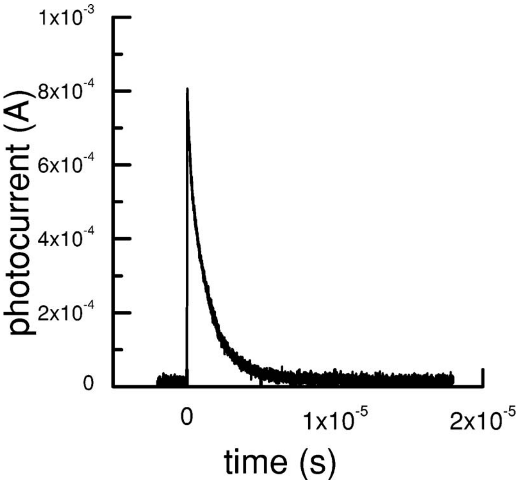

FIG. 4. Time-of-flight photocurrent on a linear scale for a 400 nm thick TiO_2 sample at an applied bias of 2.5 V.

IV. DISCUSSION

From the charge extraction measurements a capacitance of 8×10^{-7} F cm^{-2} is found. When comparing this capacitance with a parallel plate capacitance with a dielectric constant of 10 (for $CuInS_2$), a thickness of about 10 nm is found, which is well below the thickness of the TiO_2 and $CuInS_2$ films. We conclude that this huge capacitance is not due to space charge formation, but is related to the presence of a high density of interface states. This indicates that storage of charge in interface states is substantial and cannot be neglected. Furthermore, the donor and acceptor densities found for TiO_2 and $CuInS_2$ are $N_d=10^{17}$ and $N_a=10^{16}$, respectively,

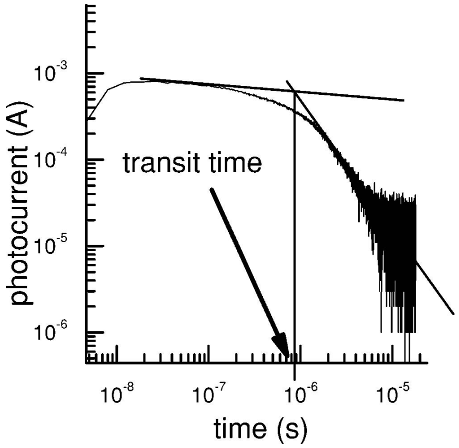

FIG. 5. Time-of-flight photocurrent from Fig. 4 on a log-log scale. The transit time is found from the intersects of the tangents .

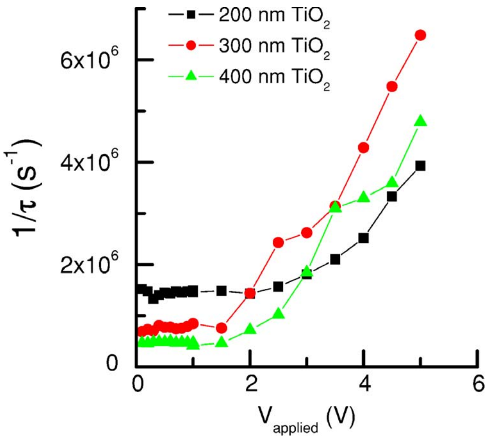

FIG. 6. (Color online) The transit time as a function of the applied voltage for 200, 300, and 400 nm thick TiO_2 samples.

as has been determined in previous investigations.[14] Therefore, we cannot expect that full depletion is reached in the TiO_2 films at the applied voltages. Accordingly, the assumption that the electric field is constant throughout the TiO_2 layer cannot be made in our case.

In order to interpret the TOF results a model is developed for the potential distribution in a *pn* junction with interface states and with one of the components ($CuInS_2$) in full depletion. Next, a charge transport model is developed, in which the inhomogeneous electric field is incorporated. With the aid of these models the TOF results can be explained accurately. By fitting the model parameters to the TOF response, it is possible to determine the concentration and the neutrality level of the interface states, which is of paramount importance for understanding the device physics of CIS-based solar cells.

A. Electrostatic model

In the present configuration, the applied voltage V is distributed over the TiO_2 and $CuInS_2$ films according to

$$V = \phi_n + \phi_p, \tag{3}$$

in which ϕ_n and ϕ_p are the potential drops over the TiO_2 film and the $CuInS_2$ film, respectively. In analogy with Rau *et al.*,[10,11,15] a model is elaborated in which interface states determine the distribution of the potential drop over the TiO_2 and the $CuInS_2$. The model is presented in Fig. 7. Following Rau *et al.*,[10,11,15] we assume that the interface-state occupation is determined by the Fermi level in the $CuInS_2$ and that the interface state density N_i (number of states per area per energy unit) is constant. Four charges are relevant in this model: Q_{Au}, Q_{CIS}, Q_i, and Q_{TiO_2}, which are the charges in the gold backcontact, the fully depleted $CuInS_2$, the interface states, and the TiO_2, respectively. The charge of the interface states, Q_i, shown schematically in the lower part of Fig. 7, is given by

$$Q_i = qN_i(qV + E_{g,p} - \Delta E_{F,n} - \phi_0), \tag{4}$$

in which q is the elementary charge, N_i is the interface states density, ϕ_0 is the neutrality level of the interface states in electron-volts (eV), $E_{g,p}$ is the band gap of the $CuInS_2$, V is the applied bias, and $\Delta E_{F,n}$ is the difference between the Fermi level in the TiO_2 and the conduction band of the $CuInS_2$, as can be seen in Fig. 7. Charge neutrality implies

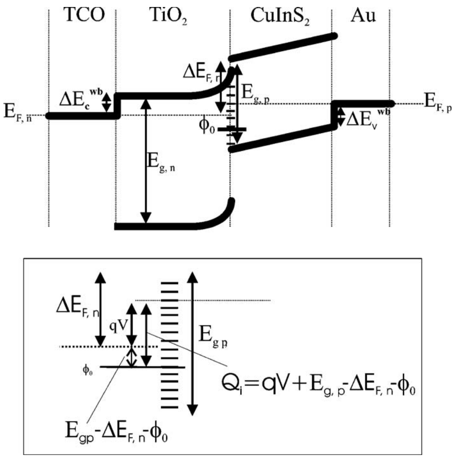

FIG. 7. Electrostatic model of the $TiO_2/CuInS_2$ heterojunction. The potential distribution is governed by the population of the interface states.

$$Q_{\mathrm{Au}} + Q_{\mathrm{CIS}} + Q_i + Q_{\mathrm{TiO}_2} = 0, \tag{5}$$

i.e.,

$$Q_{\mathrm{Au}} - qN_a d_p + qN_i(qV + E_{g,p} - \Delta E_{F,n} - \phi_0) + (2q\varepsilon_n N_d)^{1/2}\left(\phi_n - \frac{kT}{q}\right)^{1/2} = 0, \tag{6}$$

in which d_p is the thickness of the $CuInS_2$ layer, ε_n is the dielectric constant of anastase TiO_2, k is the Boltzmann's constant, and T is the temperature in Kelvin. A closed energy sum can be constructed if one assumes that the Fermi levels are flat in the *n*-and *p*-type materials. The applied bias relates to a rise in the Fermi level with qV. Starting at the Fermi level in the gold contact, first the energy is lowered by the valence band offset ΔE_v^{wb} and the potential drop across the fully depleted $CuInS_2$. Next, the energy rises with $E_{g,p}$ to reach the $CuInS_2$ conduction band. Upon lowering the energy with $\Delta E_{F,n}$ one meets the TiO_2 Fermi level. Finally, raising the energy with qV the $CuInS_2$ Fermi level is reached. This is expressed in the following equations:

$$-\Delta E_v^{wb} - \frac{qN_A d_p^2}{2\varepsilon_p} + \frac{Q_{\mathrm{Au}} d_p}{\varepsilon_p} + E_{g,p} - \Delta E_{F,n} + qV = 0, \tag{7a}$$

$$-\Delta E_v^{wb} - q\phi_p + E_{g,p} - \Delta E_{F,n} + qV = 0, \tag{7b}$$

in which ε_p is the dielectric constant of $CuInS_2$. From Eqs. (7a) and (7b), the charge on the backcontact can be derived according to

$$Q_{\mathrm{Au}} = \left(\Delta E_v^{wb} + \frac{qN_A d_p^2}{2\varepsilon_p} - E_{g,p} + \Delta E_{F,n} - qV\right)\frac{\varepsilon_p}{d_p}. \tag{8}$$

Similarly, an expression for $\Delta E_{F,n}$ can be derived from Eq. (7b), leading to

$$\Delta E_{F,n} = -q\phi_p + qV + E_{g,p} - \Delta E_v^{wb}. \tag{9}$$

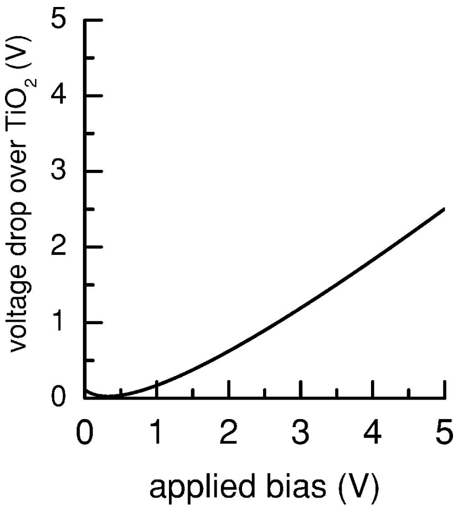

FIG. 8. Calculated voltage drop over a 300 nm thick TiO_2 film as a function of the applied bias. $N_i=10^{12}$ cm^{-2}.

Upon the substitution of Eqs. (7a), (7b), and (9) into Eq. (6), ϕ_n and ϕ_p can be calculated for every applied bias voltage with the interface states density as parameter.

A maximum value for N_i is derived from the capacitance C, which is found with the charge extraction method. From Eq. (4) it follows:

$$C = \frac{dQ_i}{dV} = \frac{d[qN_i(qV + E_{g,p} - \Delta E_{F,n} - \phi_0)]}{dV} = \frac{d(q^2VN_i)}{dV} = q^2N_i = 8 \times 10^{-7}\ \text{F/cm}^2. \quad (10)$$

The interface state density that follows from this formula has the units J^{-1} cm^{-2} and one must divide this by q to calculate the interface states per eV. We find an interface states density of 2.5×10^{12} cm^{-2} eV^{-1}.

Figure 8 presents the voltage drop over the TiO_2 film as a function of the applied bias V with $N_i=2.5\times10^{12}$ cm^{-2} eV^{-1}. Other parameters are: $N_a=10^{16}$ cm^{-3}, $N_d=2\times10^{17}$ cm^{-3}, $\phi_0=0.3$ eV, $d_p=500$ nm, $E_{g,p}=1.55$ eV, $\Delta E_v^{wb}=0.1$ eV, $\varepsilon_n=55$, and $T=293$ K. Figure 8 reveals that the voltage drop over the TiO_2 film has a similar appearance as the TOF plot in Fig. 6, i.e., for low applied bias voltages the potential drop over the TiO_2 film remains almost constant. This implies that Fermi-level pinning in the TiO_2 is responsible for the TOF behavior of the samples, as will further be discussed later. Moreover, the small voltage drop in the TiO_2 film confirms that the TiO_2 film does not reach full depletion in the TOF experiments.

B. Charge transport model

In TOF experiments on $TiO_2/CuInS_2$ heterojunctions, the voltage drop over the TiO_2 film establishes an electric field, which is a driving force for electron transport. However, as discussed earlier, TiO_2 does not reach full depletion during the TOF experiment. Following the approach by Emelianova *et al.*,[16] the TiO_2 layer is divided into two regions, a depletion region w, in which the potential drop occurs, and a neutral region d-w. The depletion width w of the space-charge region in TiO_2 is given by

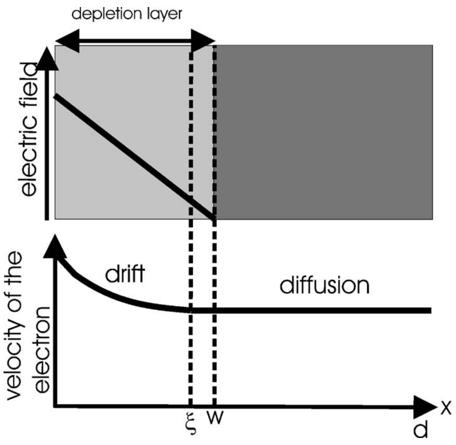

FIG. 9. Schematic representation of the electric field and electron velocity in the TiO_2. The electric field drops linearly over the depletion region. At ξ, which lies within the depletion region, the velocity becomes diffusion dominated.

$$w = \sqrt{\frac{2\varepsilon_n\phi_n}{qN_d}}. \quad (11)$$

In the present experiment, the electrons cross the TiO_2 with a velocity

$$v = v_{\text{drift}} + v_{\text{diff}}, \quad (12)$$

in which v_{drift} is the drift velocity and v_{diff} is the diffusion velocity. In the depletion layer the electron velocity is dominated by v_{drift}. The electric field, E, in the depletion region is a function of the distance x from the junction and reads

$$E(x) = \frac{qN_d}{\varepsilon_n}(w - x). \quad (13)$$

As indicated in Fig. 9, the electric field drops linearly from qN_dw/ε_n at the surface to zero in the bulk. Accordingly, the drift velocity v_{drift} is given by

$$v_{\text{drift}}(x) = \mu E(x) = \frac{\mu qN_d}{\varepsilon_n}(w - x) \quad (14)$$

and also decreases with x until it equals the diffusion velocity at ξ. At this point, a change from drift-dominated to diffusion-dominated electron transport occurs. In Fig. 9 the division of TiO_2 in a drift-dominated and a diffusion-dominated region is shown. The point ξ, where diffusion takes over, lies close to the depletion region edge.

The earlier model can be used to explain the TOF results. The transit time for the drift component is found by integrating Eq. (14) from $x=0$ to $x=\xi$ (see Fig. 9) and yields

$$\tau_{\text{drift}} = \int_{x=0}^{x=\xi} \frac{\mu qN_d}{\varepsilon_n}(w - x) = \frac{\varepsilon_n}{\mu qN_d}\ln\left(\frac{w}{w-\xi}\right). \quad (15)$$

According to the Einstein equation, the diffusion transit time equals

$$\tau_{\text{diff}} = \frac{(d-\xi)^2}{2D} = \frac{(d-\xi)^2 q}{2\mu kT}. \quad (16)$$

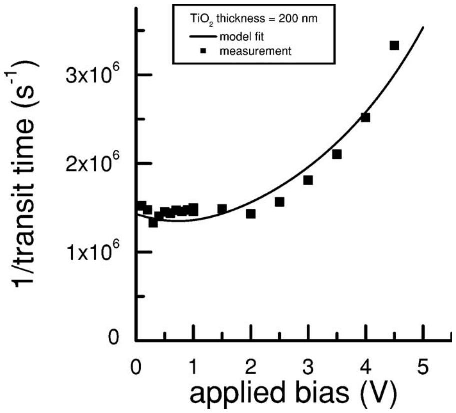

FIG. 10. Calculated (line) and measured (squares) TOF response for the 200 nm thick TiO$_2$ film.

The total transit time τ is the sum of τ_{drift} and τ_{diff}

$$\tau = \frac{1}{\mu}\left[\frac{\varepsilon_n}{qN_d}\ln\left(\frac{w}{w-\xi}\right) + \frac{(d-\xi)^2 q}{2kT}\right]. \qquad (17)$$

Since w is related to ϕ_n and ξ is related to w, ϕ_n actually determines the value of τ in Eq. (17).

C. Combining the models and fitting the TOF experiments

Equation (17), in combination with ϕ_n obtained from the electrostatic model, explains the TOF results very well. The following fit parameters are used: $N_a = 10^{16}$ cm^{-3} $N_d = 2 \times 10^{17}$ cm^{-3}, $\phi_0 = 0.3$ eV, $d_p = 500$ nm, $E_{g,p} = 1.55$ eV, $\Delta E_v^{wb} = 0.1$ eV, $\varepsilon_n = 55$, and $\varepsilon_p = 10$. The remaining free parameters are the electron mobility and the interface states density. As a result of the Fermi-level pinning, the voltage drop ϕ_n is almost independent on the applied bias at low applied bias. Furthermore, because of the low value for ϕ_n, the drift component is much less than the diffusion component in most of the TiO$_2$ film, i.e., $w \ll d$. Figures 10–12 present the experimental data points and the curves obtained from the model. The agreement is good. From these fits, the electron mobility is found to be 10^{-2} cm^2 V^{-1} s^{-1} for all three TiO$_2$ film thicknesses. Furthermore, the interface states density varies substantially with the TiO$_2$ film thickness, i.e., 5×10^{11}, 2×10^{12}, and 6×10^{12} eV^{-1} cm^{-2} for 200, 300, and 400 nm thick TiO$_2$ films, respectively. Uncertainty in the found values for the mobility and the interface states density has to be considered, since two model parameters (i.e., ϕ_0 and ΔE_v^{wb}) are estimated. Within a range of 0.1–0.5 eV for both parameters, the interface state densities vary ~10% for the 200 nm thick TiO$_2$ film and 50% for the 400 nm thick TiO$_2$ film. This variation of the interface state density is of minor importance and does not affect our conclusions. The found values for the mobilities are even less dependent on the ϕ_0 and ΔE_v^{wb} estimates.

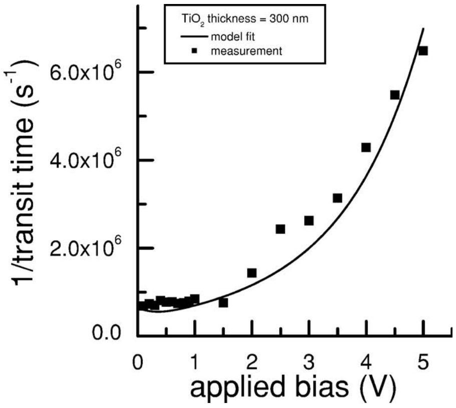

FIG. 11. Calculated (line) and measured (squares) TOF response for the 300 nm thick TiO$_2$ film.

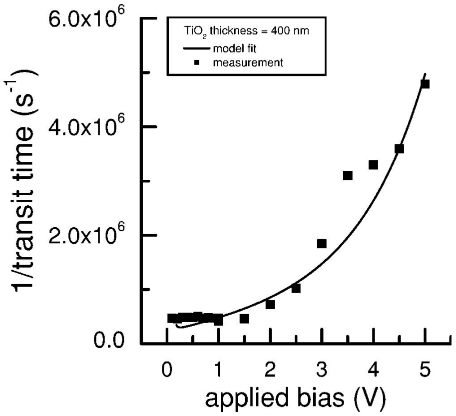

FIG. 12. Calculated (line) and measured (squares) TOF response for the 400 nm thick TiO$_2$ film.

Mobility values for electrons in TiO$_2$ in literature range from beyond 1 cm^2/V s for flat-layer TiO$_2$ to as small as 10^{-7} cm^2/V s for nanoporous TiO$_2$.[17,18] A value of 10^{-2} cm^2/V s for the electron mobility in TiO$_2$ has also been reported by Hendry *et al.*[19] for their nanoporous TiO$_2$. It is known that the process parameters of spray pyrolysis influence the surface morphology, which ranges from flat to porous.[20] The mobility found in this work indicates that the TiO$_2$ films contain some porosity, which is indeed not unexpected for spray-deposited films.

It is found in this study that an increase of the interface states density with increasing layer thickness occurs. Thicker sprayed TiO$_2$ films have more surface roughness, leading to a larger interfacial contact area. Accordingly, the concentration of interface states increases, as it had been defined as the number of states per eV per area. The interface states neutrality level is 0.3 eV above the CuInS$_2$ valance band, irrespective of the TiO$_2$ film thickness. It is concluded that a rougher surface with a larger contact area results in an increase of interface states, and a stronger pinning of the Fermi level.

V. CONCLUSIONS

This study performed TOF measurements on TiO$_2$/CuInS$_2$ heterojunctions. To allow interpretation of the data, an electrostatic model is introduced in which interface states are dominant and in which CuInS$_2$ is in full depletion. Furthermore, electron transport in TiO$_2$ has a drift and a diffusion contribution. With the aid of this model, the TOF data can be explained accurately. The concentration of interface states is found to range between 0.5×10^{12} and 6×10^{12} eV^{-1} cm^{-2}. The larger surface roughness of thicker

TiO_2 films explains this variation well. The neutrality level of these interface states is 0.3 eV above the valence band of $CuInS_2$. Finally, the electron mobility of TiO_2 is 10^{-2} cm^2 V^{-1} s^{-1} irrespective of the film thickness.

ACKNOWLEDGMENTS

Advanced Surface Technologies (Bleiswijk, the Netherlands) is acknowledged for supplying the samples. The investigations are financially supported by SenterNovem.

[1] M. Nanu, J. Schoonman, and A. Goossens, Adv. Funct. Mater. **15**, 95 (2005).
[2] M. Nanu, J. Schoonman, and A. Goossens, Nano Lett. **5**, 1716 (2005).
[3] F. Lenzmann, M. Nanu, and O. Kijatkina, Thin Solid Films **451–452**, 639 (2004).
[4] M. Krunks, O. Bijakina, and T. Varema, Thin Solid Films **338**, 125 (1999).
[5] M. Krunks, V. Mikli, and O. Bijakina, Thin Solid Films **361–362**, 61 (2000).
[6] M. Krunks, O. Kijatkina, and H. Rebane, Thin Solid Films **403–404**, 71 (2002).
[7] I. Oja, A. Mere, and M. Krunks, Solid State Phenom. **99–100**, 259 (2004).
[8] M. Krunks, O. Bijakina, and V. Mikli, Sol. Energy Mater. Sol. Cells **69**, 93 (2001).
[9] M. Nanu, J. Schoonman, and A. Goossens, Thin Solid Films **451–452**, 193 (2004).
[10] M. Turcu and U. Rau, J. Phys. Chem. Solids **64**, 1591 (2003).
[11] U. Rau, D. Braunger, R. Herberholz, H. W. Schock, J.-F. Guillemoles, L. Kronik, and D. Cahen, J. Appl. Phys. **86**, 497 (1999).
[12] W. E. Spear, J. Non-Cryst. Solids **1**, 197 (1969).
[13] H. Scher and E. W. Montroll, Phys. Rev. B **12**, 2455 (1975).
[14] R. Loef, J. Schoonman, and A. Goossens, J. Appl. Phys. **102**, 024512 (2007).
[15] U. Rau and M. Schmidt, Thin Solid Films **387**, 141 (2001).
[16] E. V. Emelianova, V. I. Arkhipov, and G. J. Adriaenssens, J. Non-Cryst. Solids **352**, 1122 (2006).
[17] T. Dittrich, Phys. Status Solidi A **182**, 447 (2000).
[18] B. van der Zanden and A. Goossens, J. Phys. Chem. B **104**, 7171 (2000).
[19] E. Hendry, M. Koeberg, and B. O'Regan, Nano Lett. **6**, 755 (2006).
[20] A. Duta, Thin Solid Films **511–512**, 195 (2006).